Pergamon

SCIENCE DIRECT®

Tetrahedron: *Asymmetry* 14 (2003) 2143–2152

TETRAHEDRON: *ASYMMETRY*

Enantioseparation of 1-(*p*-bromophenyl)ethanol by crystallization of host–guest complexes with permethylated β-cyclodextrin: crystal structures and mechanisms of chiral recognition

Arnaud Grandeury,[a] Samuel Petit,[a,*] Géraldine Gouhier,[b] Valérie Agasse[a] and Gérard Coquerel[a]

[a]*Sciences et Méthodes Séparatives (SMS), UPRES EA 2659, IRCOF-Université de Rouen, F-76821 Mont Saint-Aignan Cedex, France*

[b]*Laboratoire des Fonctions Azotées et Oxygénées Complexes, UMR 6014, IRCOF-Université de Rouen, F-76821 Mont Saint-Aignan Cedex, France*

Received 10 April 2003; accepted 25 April 2003

Abstract—It is shown that racemic 1-(*p*-bromophenyl)ethanol (*p*-Br-PE) can be quantitatively resolved by successive recrystallizations of (1:1) supramolecular complexes formed with permethylated β-cyclodextrin (TMβ-CD). The two enantiomerically pure complexes were characterized by physical methods and their crystal structures were determined. The comparison of both inclusion geometries and packing modes in these structures revealed distinct structural features allowing the enantioseparation of the guest to be understood. Chiral discrimination mechanisms are discussed in terms of the capability of TMβ-CD to induce the formation of stereospecific host–guest complexes by simple crystallization in aqueous medium.

1. Introduction

Cyclodextrins (CDs) are cyclomaltooligosaccharides obtained by enzymatic degradation of starch.[1] The most common CDs are composed of six, seven or eight α-D-glucopyranose units (α-, β-, γ-CD, respectively), linked by α-(1→4) glycosidic bonds.[2] These macrocyclic compounds present a toroidal shape, and their hollow structure enables them to host a large variety of small guest molecules, leading to supramolecular complexes.[3] The driving force of the formation of these inclusion complexes can involve several types of intermolecular interactions such as hydrogen bonds, van der Waals forces, hydrophobic interactions, strain energy of the macrocycle ring or dipolar interactions.[4,5]

Because of their weak toxicity, CDs are widely used in pharmaceutical, cosmetology and food industries, mainly to improve the dissolution behaviour of poorly soluble organic compounds in aqueous medium, to increase bioavailability, or to protect their guest from chemical degradation.[6]

Natural cyclodextrins can be chemically modified in order to enhance some of their properties.[7,8] In particular, the full methylation of the three hydroxyl groups per glucosidic unit leads to the 2,3,6-tri-*O*-methyl derivatives (TM-CDs), and TMβ-CD is the most widely used chiral selector for the preparation of gas chromatography columns.[9]

By contrast with the numerous publications dealing with the use of CDs for enantioseparation on an analytical scale (mainly chromatography and capillary electrophoresis),[2] only a few papers have reported the possible chiral discrimination of racemic mixtures by crystallization of inclusion compounds with CDs.[10–14] In some cases, crystal structures have provided valuable data for the understanding of chiral recognition mechanism(s).[15–17] The poor ability of native CDs to achieve enantioseparation of guest compounds was supposed to result from the molecular rigidity of these hosts, whereas the loss of intramolecular hydrogen bonds between hydroxyl groups in TM-CDs is assumed to improve their capability for chiral recognition. Indeed, this higher selectivity was explained on a structural basis by the higher molecular flexibity of these derivatives, which is assumed to allow a conformational adjustment to each enantiomer ('induced-fit').[17,18]

* Corresponding author. Tel.: +33-(0)2-35522428; fax: +33-(0)2-35522959; e-mail: samuel.petit@univ-rouen.fr

0957-4166/$ - see front matter © 2003 Elsevier Ltd. All rights reserved.
doi:10.1016/S0957-4166(03)00360-4

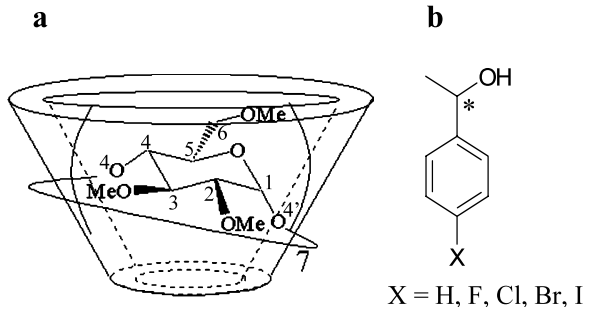

Figure 1. Molecular structures of tri-*O*-methylated-β-cyclodextrin (TMβ-CD, a) and *p*-halogenated derivatives of phenylethanol (*p*-X-PE, b)

Since we are interested in trying to understand some fundamental aspects of chiral discrimination by means of supramolecular complexation with TMβ-CD (Fig. 1a), we have undertaken a systematic study of the crystallization behaviour of host–guest complexes formed between this host and a homologous series of racemic *p*-halogenated derivatives of 1-phenylethanol (Fig. 1b). The choice of these guests as model compounds allows the possible enantioseparation and the relative influence of the chemical nature of a halogenated substituent located far from the stereogenic center to be investigated simultaneously. Our preliminary results[19] have revealed that some enantioenrichment occurred for all these derivatives, but with a large diversity of enantiomeric excess (e.e.) values in solid state samples. Furthermore, the partial resolution induced by crystallization was shown to be highly sensitive to kinetic parameters since the obtained e.e. are in most cases strongly affected by crystallization durations. Owing to this unexpected diversity observed among a series of homologous guest compounds, we are now interested in reaching more detailed data regarding the crystalline phases behaving as diastereomeric compounds.

The present paper reports the preparation, the characterization and the crystal structure determination of supramolecular complexes formed between TMβ-CD and the two enantiomers of *p*-bromophenylethanol (*p*-Br-PE). These data are discussed in terms of chiral recognition mechanisms, and a comparative analysis of our results with reference to that deduced from previously published crystal structures is presented.

2. Results

2.1. Resolution of racemic *p*-Br-PE by formation of solid state complexes with TMβ-CD

The ability of TMβ-CD to discriminate partially the two enantiomers of *p*-Br-PE by means of a simple crystallization procedure was established recently.[19] The (1:1) stoichiometry of the obtained solid state supramolecular complex was determined from NMR analyses, and its characterization by XRPD revealed its satisfactory crystallinity. Furthermore, it was shown that a high e.e. of *p*-Br-PE (about 70%) could be reached when filtration was performed less than 10 min after the appearance of the first crystals. If crystallization was allowed to proceed for 1 h, the e.e. within solid state samples decreased to about 12%, and e.e. values as low as 6% were measured when the suspension was maintained under stirring for 3 h. Simultaneously, the amount of collected solid increased significantly, showing that improving the crystallization yield is detrimental to chiral discrimination.

The above data were used in order to design an optimal procedure aiming at separating the two enantiomers of *p*-Br-PE. Starting from large amounts (ca. 0.7 mmol) of host and guest compounds, successive recrystallizations were performed and solid samples were collected by filtration after 1 h of crystallization under stirring, so that satisfactory yields could be reached. Figure 2 presents simultaneously the evolution of the e.e. of *p*-Br-PE within the obtained solid samples and the global crystallization yield for the successive recrystallizations. It appears that a pure enantiomer can be reached after six runs, with a very low global yield. Nevertheless, recycling of mother liquors appeared easy to perform, and allowed to obtain the two enantiomers with high yields (>90%).

2.2. Physical characterization of host–guest complexes

The two crystalline complexes containing each of the pure enantiomers were characterized by XRPD and DSC. The absolute configuration of the guest compounds were determined from crystal structures (see below), so that the two complexes are identified hereafter according to the included enantiomer. It can be seen from Figure 3 that XRPD patterns exhibit distinct features, probably associated to different crystal packings. The DSC curves of these complexes are shown in Figure 4 and indicate that the thermal behaviour of the complex containing the (*S*) enantiomer of *p*-Br-PE is characterized by a single endothermic phenomenon at 154°C (onset, ±1°C) whereas the DSC curve of the complex made of TMβ-CD and (*R*)-*p*-Br-PE exhibits two successive thermal events at 147 and 158°C (onsettemperatures, ±1°C). Thermomicroscopy observations performed at the same heating rate (data not shown) have indicated that this complex undergoes a succession of fusion/recrystallization/fusion phenomena.

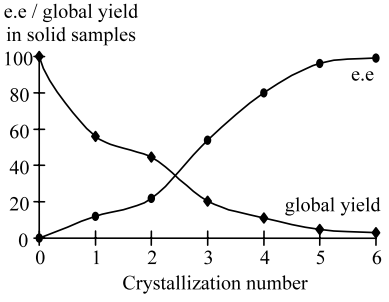

Figure 2. Evolution of e.e. of the guest and of the global yield obtained by successive recrystallizations of *p*-bromophenylethanol/TMβ-CD complexes.

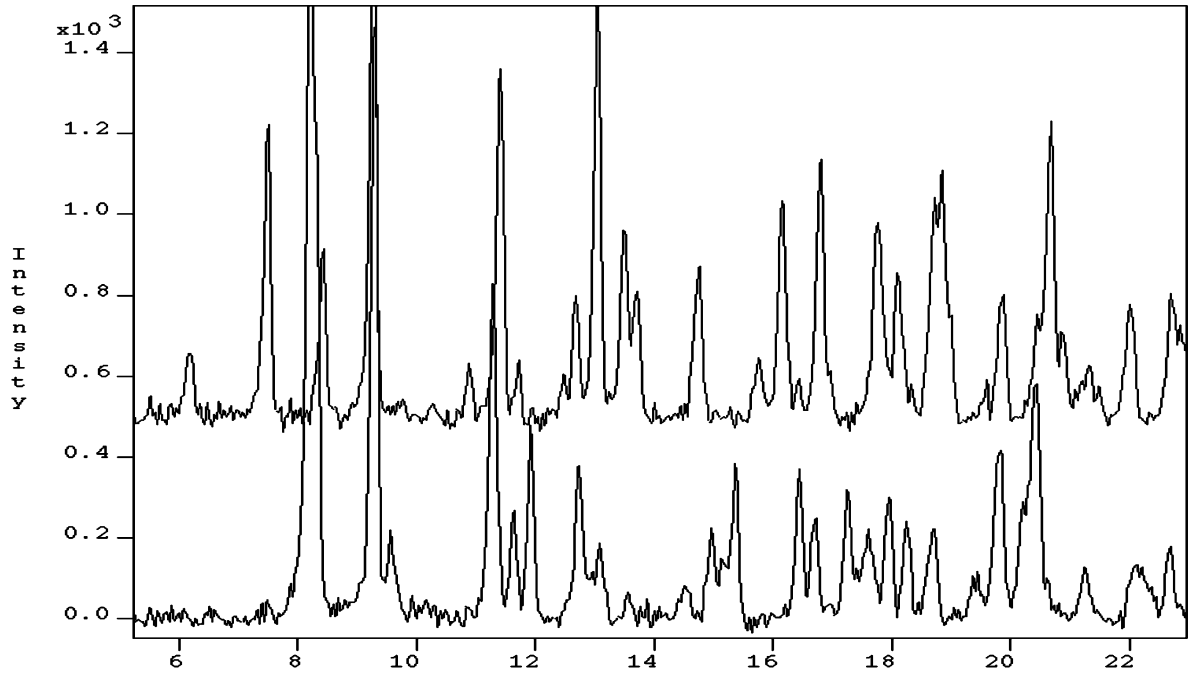

Figure 3. XRPD patterns of the complexes formed between TMβ-CD and the two enantiomers of *p*-bromophenylethanol (upper: TMβ-CD/(*S*)-*p*-Br-PE; lower: TMβ-CD/(*R*)-*p*-Br-PE).

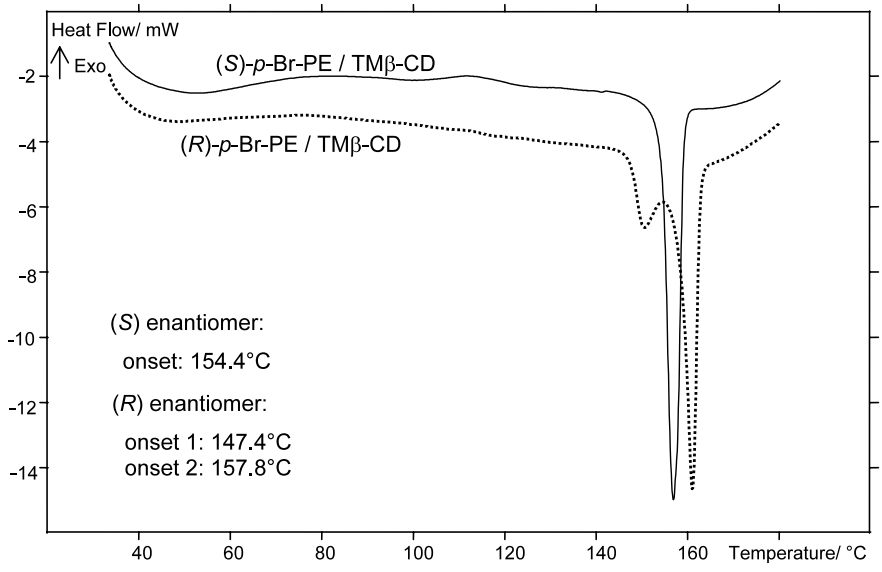

Figure 4. DSC curves for the complexes formed between TMβ-CD and the two enantiomers of *p*-bromophenylethanol.

The physical characterization of the two complexes was completed by solubility measurements, determined at 40°C in water by using the gravimetric method. The obtained values (1.2 and 2.4% w/w for the complexes including (*S*)- and (*R*)-*p*-Br-PE, respectively) are significantly different, in consistency with the existence of distinct crystalline phases for these two complexes.

2.3. Crystal growth investigations and structure determinations

In order to get deeper insights into the mechanisms of chiral discrimination, crystal structures of the two complexes characterized above were determined by X-ray diffraction on single crystals. Although these crystals could be prepared from pure enantiomers, it was of interest to study the evolution of enantioenrichment in close-to-equilibrium conditions. It was therefore decided to perform crystal growth investigations at 40°C from a solution containing a (1:1) stoichiometry of TMβ-CD and racemic *p*-Br-PE. From such a slightly supersaturated solution, the first crystals obtained presented an acicular morphology (Fig. 5a). These crystals were carefully picked up from the mother liquor for GC analyses, and the solution was maintained supersaturated in order to obtain new crystals which were also

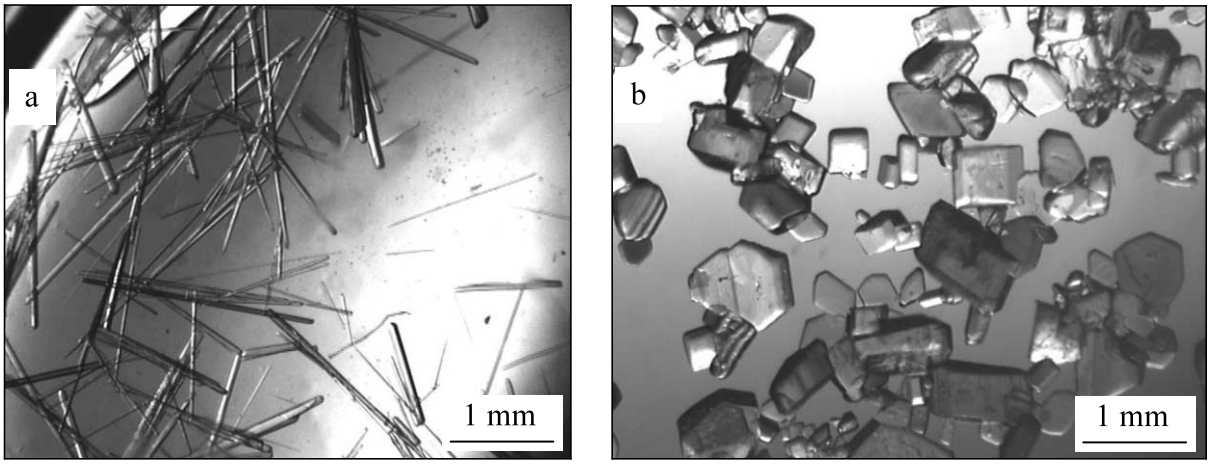

Figure 5. Photographs of single crystals obtained successively from a saturated solution at 40°C containing TMβ-CD and the two enantiomers of *p*-bromophenylethanol.

sorted out from the growth medium. This procedure was repeated over several days, and GC analyses of *p*-Br-PE contained in these crystals revealed no significant evolution of enantiomeric excesses (ca. 80% of the (*S*) enantiomer). After 5 days, crystals exhibiting a distinct morphology (prismatic shape, Fig. 5b) also appeared in the solution, and were shown to contain an almost constant e.e. close to 40%, with an excess of the (*R*) enantiomer. After 7 days, crystals of the acicular morphology did not form any more, and prismatic crystals only could be collected during the following days. Well-defined single crystals selected from each of these two morphological families were used for structural investigations.

Crystal data and experimental details of X-ray diffraction analyses are reported in Section 5. Most of the non-hydrogen atoms of the 7 glucosidic moieties could be identified by resolution with direct methods. Successive refinements and analyses of difference electron density maps allowed to locate both missing atoms of TMβ-CD and the *p*-Br-PE molecules. Although single crystals were not enantiomerically pure (see above), no residual peak corresponding to counter enantiomer molecules could be identified in the final refinement steps. The final *R* factor obtained for the complex formed with the (*R*) enantiomer of *p*-Br-PE is significantly higher than that reached for the (*S*) enantiomer. It was suspected that this could be due to the presence of disordered water molecules within the crystal lattice, but this hypothesis could not be assessed in a satisfactory way during the last stages of refinement. Superimpositions of XRPD patterns simulated from crystal structures with experimental ones allowed to establish the representativity of single crystals.

2.4. Description of crystal structures

Bond lengths and angles of TMβ-CD in the two structures agree with usual values, and all glucosidic residues exhibit the $^4C_1$ chair conformation often observed in related structures.[20] Superimposition of the two macrocycles shows that molecular conformations are similar, and it can be seen from Figure 6 that the only significant differences deal with the orientation of the methoxy groups. Further comparison between the host conformations can be derived from Table 1, which summarizes the tilt angle values (dihedral angles between the O4 mean plane and the plane defined by C1, C4, O4 and O4′ atoms of each residue, see Fig. 1a) measured in the present structures and in previous studies.[16,21–30] Table 1 also reports crystallographic parameters, from which it appears that the unit-cell dimensions obtained in the structures of TMβ-CD/*p*-Br-PE complexes constitute original data.

The molecular geometry of guest compounds is in agreement with standard values, and the absolute configuration of the enantiomer included in each of the

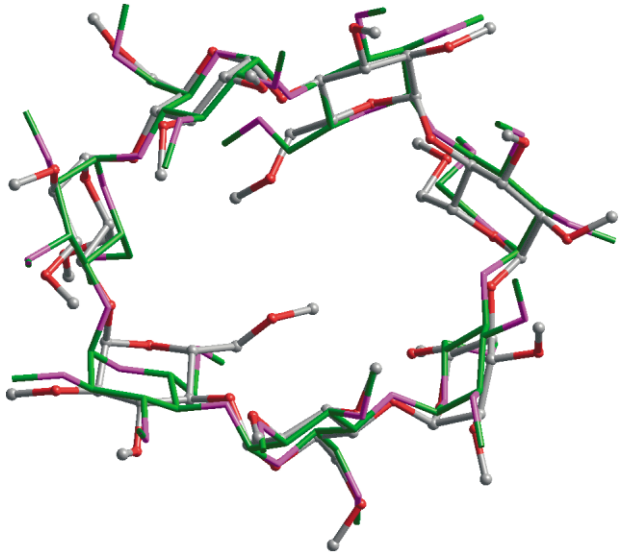

Figure 6. Superimposition of the macrocyclic hosts in the crystal structures of the complexes formed between TMβ-CD and the two enantiomers of *p*-bromophenylethanol (hydrogen atoms are omitted for clarity).

Table 1. Comparison of crystallographic parameters and tilt angle values in the present structures and in previously determined crystal structures containing TMβ-CD[a]

Code[b]	Crystallographic parameters			Molecular conformation (tilt angle values, °)							Ref.
	a (Å)	*b* (Å)	*c* (Å)	G1	G2	G3	G4	G5	G6	G7	
(*S*)-*p*-Br-PE	15.113	15.223	35.876	32.1	21.7	−15.8	54.6	29.0	−16.3	38.7	This work
(*R*)-*p*-Br-PE	10.563	14.731	27.355	26.1	12.7	−11.5	32.9	43.1	−17.3	46.1	This work
PIP	14.997	21.368	28.205	30.4	16.7	−12.7	43.0	34.9	−16.3	42.4	21
SFP	15.271	21.451	27.895	26.5	18.6	−12.3	43.3	34.5	−14.3	36.6	22
RFP	15.092	21.714	28.269	30.2	14.5	−12.5	43.8	36.4	−12.9	42.2	22
MIP	15.669	20.798	25.486	27.8	13.2	6.0	46.6	28.3	−13.6	51.7	23
BPA	14.890	21.407	28.540	28.2	15.8	−14	43.4	36.6	−14.5	41.3	23
ELR	14.796	22.444	27.720	31.9	12.8	−14	37.9	35.8	−13.8	38.7	24
SNP	15.179	21.407	27.67	26.9	20.7	−9.3	44.3	34.5	−14.4	34.4	25
SIP	15.232	21.327	27.597	28.3	18.8	−11.2	41.9	33.3	−14.2	36.4	26
MTC	14.818	19.362	26.51	37.9	21.0	−4.6	72.9	57.3	−24.5	24.7	27
LMT	11.060	26.138	29.669	26.5	10.2	−7.4	47.7	25.1	−9.3	46.5	28
MCH	11.149	25.664	29.427	15.7	6.0	51.7	8.9	24.8	8.4	40.1	29
RDM	11.190	26.08	29.187	16.1	7.2	51.3	7.3	25.7	7.7	38.7	30
SDU	10.936	25.53	29.64	13.7	27.3	56.9	7.7	27.33	41.0	6.4	16

[a] Space group is orthorhombic $P2_12_12_1$ for all these structures except for (*R*)-*p*-Br-PE which corresponds to a monoclinic $P2_1$ system, with a β angle 98.46°.

[b] Codes of guest compounds are defined in the text (see Section 3.2).

two complexes could be identified unambiguously since the configuration of TMβ-CD is obviously established.

In both structures, the main intermolecular interaction is a hydrogen bond formed between hydroxy groups of *p*-Br-PE molecules and an oxygen atom O3 of a methoxy group. The distance between oxygen atoms is 2.98 Å for TMβ-CD/(*S*)-*p*-Br-PE and 2.80 Å for TMβ-CD/(*R*)-*p*-Br-PE. Despite similarities between the two structures in terms of macrocyclic conformation and supramolecular H-bonding, the relative orientation of host and guest components differs strongly in these complexes. Indeed, it appears from Figure 7 that the bromine atom in TMβ-CD/(*R*)-*p*-Br-PE is located at the bottom of the cavity, and the main molecular axis of *p*-Br-PE is almost parallel to the pseudo 7-axis of

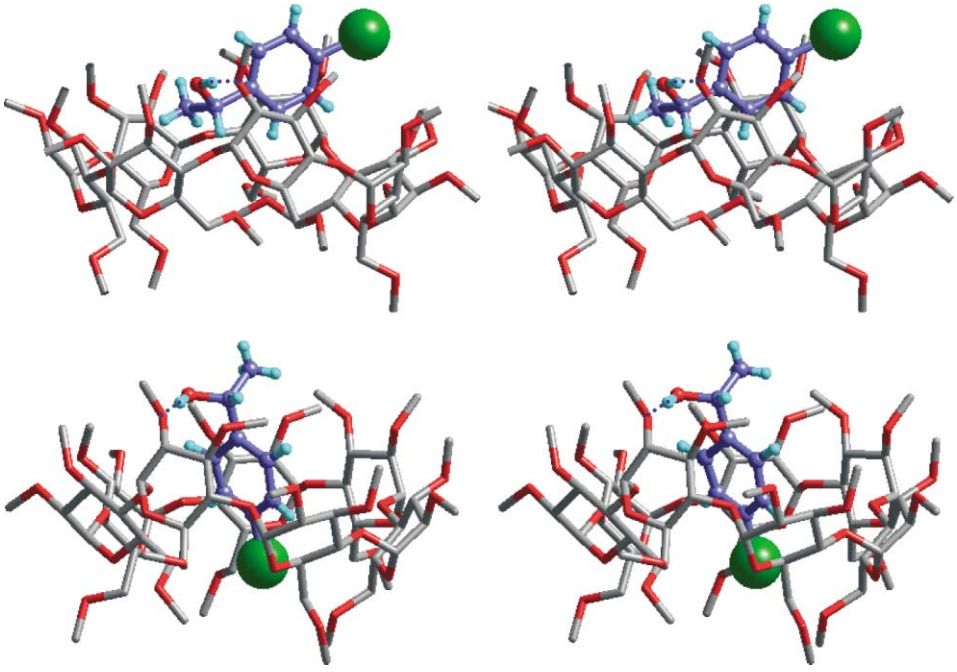

Figure 7. Stereoviews of the complexes formed between TMβ-CD and the (*S*) (upper) or the (*R*) (lower) enantiomer of *p*-bromophenylethanol (H atoms of macrocyclic hosts are omitted for clarity).

TMβ-CD, inducing that the major part of the guest molecule is engulfed in the macrocycle. By contrast, the bromine atom of (*S*)-*p*-Br-PE lies on the border of the main entrance of the macrocycle, and the aromatic moiety is therefore only partially inserted in the TMβ-CD cavity.

Figure 8 presents crystal packings of the two complexes and reveals different structural features. In the structure containing the (*S*) enantiomer, complexes are stacked according to a herringbone pattern, in connection with the 2_1 screw axis running along the *b* axis. This packing mode induces the presence of empty space between neighbouring macrocycles, which is occupied by the protruding part of guest molecules. By contrast, the crystal packing of TMβ-CD/(*R*)-*p*-Br-PE is characterized by the presence of molecular columns running along the *a* axis. These columns result from the head-to-tail stacking of complexes generated by simple translation.

2.5. Molecular modelling investigations

In order to estimate the relative energy involved in the supramolecular associations described above and to evaluate their stereoselectivity, molecular mechanics calculations were performed by using the Cerius[2] software. Atomic charges were obtained from MOPAC calculations (AM1 algorithm) interfaced with the Sybyl software. Prior to energy calculations of host–guest interactions, each complex was submitted to energy minimizations in order to ensure the validity of our modelling procedures and computations. This preliminary step allowed to confirm that the relative orientation of host and guest components observed in the two crystal structures actually correspond to energy minima. Then, the two components were separated and the interaction energy was estimated as the difference between the total relative energy of the complex and the sum of the relative energies of the isolated constituents: $E_{\text{interaction}} = E_{(\text{host+guest})} - [E_{(\text{host})} + E_{(\text{guest})}]$. The obtained values are given in Figure 9, and seem consistent with the existence of a hydrogen bond and of several van der Waals contacts between hosts and guests. Since interaction energy values are calculated by differences between relative energies, it can be estimated that the uncertainty on host–guest interactions is less than 0.5 kcal mol^{-1}. Keeping in mind that these calculations are carried out in vacuum and cannot take into account the environment of the complexes, the obtained values indicate that the complex TMβ-CD/(*S*)-*p*-Br-PE is more stable by only 0.6 kcal mol^{-1} than the complex formed with (*R*)-*p*-Br-PE. It is noteworthy that this order of relative stability is identical to that observed during crystal growth experiments.

The stereoselectivity associated with the two inclusion geometries was evaluated by substituting each guest enantiomer with the opposite enantiomer. In order to maintain as far as possible the relative host–guest orientation, this step was performed by an inversion of methyl group and hydrogen atom attached to the chiral center of *p*-Br-PE. After minimization, the supramolecular interactions were calculated according to the same procedure, and relative energy values are shown in Figure 9. For both inclusion geometries, these calculations indicate that the interaction is less favourable with the counter enantiomer by 2.7 and 0.9 kcal mol^{-1} for the (*S*)→(*R*) and (*R*)→(*S*) substitutions, respectively.

3. Discussion

3.1. Mechanism of chiral discrimination of *p*-Br-PE by complexation with TMβ-CD

The possibility of separating quantitatively the two enantiomers of *p*-Br-PE by crystallization of host–guest complexes with TMβ-CD can be analyzed in terms of crystal growth and structural results. The original crys-

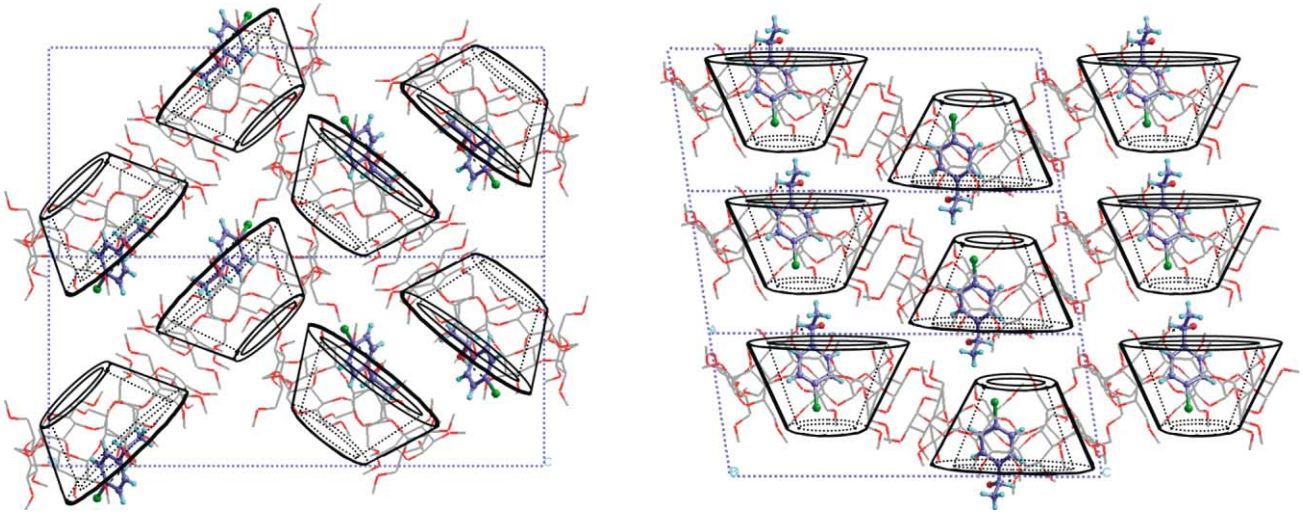

Figure 8. Projections along the *b* axis of the structures for the complexes formed between TMβ-CD and the two enantiomers of *p*-bromophenylethanol (left: TMβ-CD/(*S*)-*p*-Br-PE; right: TMβ-CD/(*R*)-*p*-Br-PE; H atoms of macrocyclic hosts are omitted for clarity).

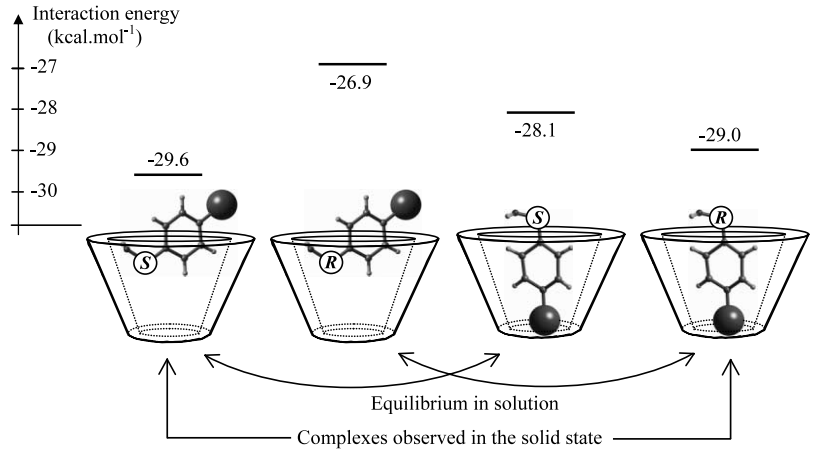

Figure 9. Schematic representation of host–guest geometries and corresponding interaction energies in the supramolecular compounds formed between TMβ-CD and the two enantiomers of *p*-bromophenylethanol, obtained by molecular modelling calculations.

tal growth procedure described in Section 2.3 indicates that stereodifferentiation results from the existence of two distinct crystalline phases behaving as diastereomeric compounds. Although these phases could be isolated and characterized by physical methods, it appeared that close-to-equilibrium growth conditions do not lead to enantiomerically pure crystals. The presence of a constant proportion of the opposite enantiomer in single crystals prepared from solutions containing a quasi-racemic composition of guest molecules indicates that each crystalline phase is able to incorporate a certain amount of complexes containing the 'wrong' enantiomer. This reveals the probable existence of solid solutions since no inclusion of mother liquor nor macroscopic defects were detected. These data also account for the necessity to perform several successive recrystallizations in order to reach pure enantiomers. Furthermore, the possibility to improve the stereoselectivity by adjusting the diffusion rate in the growth medium, for instance through an adapted stirring mode,[31] is probably of limited applicability in the present situation.

Structural data deduced from single crystal X-ray diffraction, combined with molecular modelling investigations, provide detailed information for deeper insights into the mechanisms of chiral discrimination. The comparison between inclusion geometries in the structures of *p*-Br-PE/TMβ-CD complexes indicates that stereodifferenciation induced by crystallization is associated to large differences in terms of host–guest relative orientation which could also be favoured in the solvated state. Molecular mechanics calculations cannot take into account the effect of the surrounding medium, but indicate that, in vacuum, the energy gain due to supramolecular interactions is larger for the (*S*) enantiomer than for the (*R*) enantiomer of *p*-Br-PE by about 0.6 kcal mol^{-1} (Fig. 9). More interestingly, our modelling work revealed that the stability of host–guest associations decreases significantly when the counter enantiomer is considered for each of the two inclusion geometries. Furthermore, the larger energy difference obtained in the case of a (*S*)→(*R*) replacement compared to the (*S*)→(*R*) substitution (2.7 and 0.9 kcal mol^{-1}, respectively, see Fig. 9) could account for the higher selectivity associated to this inclusion geometry. Indeed, starting from a solution containing a 50/50 mixture of *p*-Br-PE, the e.e. measured in single crystals of the orthorhombic phase could reach about 80%, whereas single crystals of the monoclinic form prepared in similar conditions usually contain an e.e. of about 40%.

These results reinforce the hypothesis of the existence in solution of a pre-chiral discrimination due to the presence of inclusion complexes exhibiting distinct geometrical features. Crystallization might act as an amplifier of the weak chiral discrimination existing between solvated inclusion complexes. The cooperative mechanisms involved in crystallization processes could actually shift the equilibria highlighted in Figure 9 between solvated species, which is consistent with the improved chiral discrimination obtained by slow crystallization experiments.

Hence, in connection with the significant difference between solubility values, the crystallization of each phase incorporating mainly one type of complex occurs, and stereodifferenciation during crystallization is likely to result from the ability of each crystal packing to recognize the complex including the suitable enantiomer during nucleation and growth steps. However, the similarities between the two macrocyclic conformations, on the one hand, and the limited magnitude of calculated energy differences resulting from enantiomeric inversions of guests, on the other hand, are consistent with the formation of solid solutions. It can also be envisaged that the insertion of complexes containing the counter enantiomer with the same inclusion geometry as the majority of the guest molecules could stabilize the crystal packing (stable solid solution).

3.2. Structural aspects of molecular and chiral recognition with TMβ-CD

To our knowledge, the relative orientation of host and guest components depicted in the structure of TMβ-CD/(*S*)-*p*-Br-PE has never been observed in complexes containing TMβ-CD, since aromatic moieties are usually engulfed within macrocyclic moieties.[17] In order to investigate further the structural features of such complexes, we have collected all published structural data (retrieved, for most of them, from the Cambridge CSD, see Cardinael et al.[30] for refcodes), and a comparative analysis revealed that these 13 structures could be classified in distinct groups, since similar unit-cell dimensions and tilt angle values were obtained for several structures. Table 1 summarizes these data, and allows to characterize the structural groups (SG) defined hereafter.

A first group, labelled SG-A, contains 8 structures which present similar features in terms of crystallographic parameters and conformations of the macrocyclic moieties, as can be seen from the comparison of tilt angles.[30] The guest compounds in these structures are *p*-iodophenol (PIP),[21] (*R*)- and (*S*)-Flurbiprofen (RFP and SFP),[22] *m*-iodophenol (MIP) and 4-biphenylacetic acid (BPA),[23] ethyl laurate (ELR),[24] (*S*)-Naproxen (SNP),[25] (*S*)-Ibuprofen (SIP),[26] and the corresponding packings were described as a head-to-tail zig–zag channel-type structure.[17] Despite a large diversity of guest compounds, the comparison of inclusion geometries within SG-A revealed similar locations and orientations of guests within the macrocycles.

A second structural group (SG-B) contains 3 members and is constituted, owing to the crystallographic parameters and macrocyclic conformations, by the complexes formed with methylcyclohexane (MCH),[29] the (*S*)-enantiomer of 1,7-dioxaspiro[5.5]undecane (SDU)[16] and the (*R*)-enantiomer of 1,3-dimethyl-5-ethyl-5-methylhydantoin (RDM).[30]

The two remaining structures correspond to particular cases: the monohydrated form of TMβ-CD (MTC) exhibits an unusual, highly distorted macrocyclic conformation,[17,27] and the complex formed with L-menthol (LMT)[28] belongs to SG-A in terms of macrocyclic conformation but to SG-B regarding its crystallographic parameters.

Hence, it appears that an important diversity exists among supramolecular complexes formed with TMβ-CD, since the two original crystal structures depicted here with *p*-Br-PE are likely to constitute prototypes of new structural groups of these complexes. The only previous study in which the structures of the complexes formed between TMβ-CD and the two enantiomers of a same compound is the case of Flurbiprofen.[22] The high similarity between the two structures led to the assumption that supramolecular complexation with TMβ-CD was not suitable for chiral discrimination.[17]

In the present situation, the crystallization mechanisms described above imply that different inclusion modes in solution induce the ability of each crystalline phase to impede, at least to a certain extent, the insertion within the crystal lattice of complexes containing the counter enantiomer. In order to assess this mechanism, NMR spectroscopy in solution (ROESY studies) will be applied. Further crystal growth and structural investigations are also in progress with other *p*-halogenated PE derivatives in order to confirm the influence of inclusion modes on chiral discrimination during the crystallization of host–guest supramolecular compounds with TMβ-CD.

4. Conclusion

Despite the probable existence of partial (stable or metastable) solid solutions, the crystallization of supramolecular complexes formed between tri-*O*-methylated-β-cyclodextrin (TMβ-CD) and the two enantiomers of *p*-bromophenylethanol (*p*-Br-PE) allows the preparative chiral resolution of the racemic mixture, by performing successive recrystallizations and recycling of mother liquors. The characterization of the two diastereomeric compounds (TMβ-CD/(*S*)-*p*-Br-PE and TMβ-CD/(*R*)-*p*-Br-PE) revealed specific solid state properties (XRPD patterns, thermal behaviours, solubilities, crystal habits, etc.). From their structural analysis, it was shown that the possibility of separating the two guest enantiomers mainly results from important differences between inclusion geometries.

Molecular modelling investigations have shown that only small energy differences exist between the diastereomeric species, from which it can be assumed that equilibria may exist in solution. However, our experimental results indicate that crystallization is likely to act as an amplifier of these limited differences, and can therefore be used in order to perform preparative chiral discrimination.

5. Experimental

5.1. Materials

Commercial TMβ-CD of high purity (>97%) was purchased from Cyclolab Inc. (Budapest, Hungary) and used without further purification. In order to perform large scale experiments, TMβ-CD was prepared from native β-CD by using the procedure published by Schurig et al.,[32] and samples were recrystallized three times in water. Racemic 1-(*p*-bromophenyl)ethanol was obtained by reduction of the corresponding ketone.[33] Permethylation of β-CD was controlled by NMR and LC–MS, and the purity of *p*-Br-PE was checked by NMR and GC–MS.

5.2. Crystallization procedures and dissociation of complexes

Crystalline complexes were obtained from aqueous solutions containing a (1:1) molar ratio of host and guest components. After the dissolution under magnetic stirring of TMβ-CD in water at room temperature, the addition of *p*-Br-PE induced the appearance of an emulsion caused by the weak miscibility of the two liquid phases. This emulsion disappeared progressively, and the complete homogeneity observed after about 1 h indicated the probable formation of solvated supramolecular complexes.

Because of the retrograde solubility of complexes formed with TMβ-CD, crystallizations were induced by heating these solutions at 40°C (±0.5°C, using a programmable cryo-thermostat). The obtained suspensions were maintained under magnetic stirring until filtration, which were performed at the crystallization temperature in order to avoid partial dissolution. Growth of single crystals were carried out within a few days by slow evaporation of saturated solutions at the same temperature.

5.3. Analytical methods and physical characterization of solid state samples

The stoichiometry of host and guest components in solid state complexes was assessed by ^{1}H NMR spectroscopy, performed in $CDCl_3$ on a Bruker AC 300® spectrometer. Enantiomeric excesses of *p*-Br-PE were determined from chiral gas chromatography analyses. The latter were performed on a Packard 5890 instrument equipped with a Supelco Betadex® column (413 K isothermal run, injector and detector temperature 523 K, Helium carrier gas, $\mu_{opt}=30$ cm s^{-1}). In order to avoid injection of TMβ-CD, which can undergo pyrolysis in analytical conditions, host and guest components were first separated by means of a micro-chromatography process on silica gel (eluant = ethyl acetate/cyclohexane (15:85); $R_{f(p\text{-X-PE})}=0.3$–0.4; $R_{f(TM\beta\text{-CD})}=0.1$).

X-Ray powder diffraction (XRPD) patterns were recorded on a Siemens D5005® diffractometer (Cu Kα). Solubilities were determined by the gravimetric method. DSC analyses were performed with a Setaram DSC 141 apparatus (sample weight from 15 to 20 mg, heating rate 5 K min^{-1}).

5.4. X-Ray investigations and crystal data

Crystal structure determinations were carried out at 100 K by means of single crystal X-ray diffraction, using an Enraf-Nonius CAD-4 automatic diffractometer with a graphite monochromated Mo Kα radiation (0.71073 Å). The measured intensities were corrected for Lorentz and polarization effects but no absorption correction was applied. The SHELX-97 program[34] was used for resolution and refinements. Initial atomic coordinates were obtained by applying direct methods and subsequently refined by using the full-matrix least-squares techniques. All non-hydrogen atoms were refined anisotropically and hydrogen atom positions were calculated without further refinement.

Structural descriptions and molecular mechanics calculations were performed with the modelling softwares Cerius[2] (v. 4.6, Accelrys Inc., 2001) and Sybyl (v. 6.8, Tripos Ass. Inc., 2001) implemented on O2 Silicon Graphics workstations. Partial atomic charges were obtained with the AM1 algorithm of MOPAC[35] and the Dreiding II force field was used for energy calculations.[36]

5.4.1. Crystal data for TMβ-CD/(*S*)-*p*-Br-PE. ($C_{63}H_{112}O_{35}\cdot C_8H_9OBr$): $M_w=1630.6$, crystal size 0.07×0.08×0.24 mm, orthorhombic, space group $P2_12_12_1$, $a=15.113(1)$, $b=15.223(1)$, $c=35.876(3)$ Å, $V=8253(2)$ Å^3, $Z=4$, $\rho=1.312$ g cm^{-3}, $F(000)=3480$, $\mu=0.585$ mm^{-1}. The data were collected in θ range 1.76–27.88° and in *hkl* range −19–19, −20–19, −47–47; 19497 reflections were measured among which 14566 with $I>2\sigma(I)$, and 974 parameters were refined. Final *R* indices [$I>2\sigma(I)$]: $R_1=0.0651$, $wR_2=0.1514$.

5.4.2. Crystal data for TMβ-CD/(*R*)-*p*-Br-PE. ($C_{63}H_{112}O_{35}\cdot C_8H_9OBr\cdot(H_2O)_\varepsilon$): $M_w=1630.6(+18\varepsilon)$, crystal size 0.16×0.32×0.48 mm, monoclinic, space group $P2_1$, $a=10.563(1)$, $b=14.731(1)$, $c=27.355(3)$ Å, $\beta=98.46(1)°$, $V=4210(1)$ Å^3, $Z=2$, $\rho=1.286$ g cm^{-3}, $F(000)=1748$, $\mu=0.573$ mm^{-1}. The data were collected in θ range 1.57–27.88° and in *hkl* range −13–13, −19–19, −35–36; 19840 reflections were measured among which 12963 with $I>2\sigma(I)$, and 978 parameters were refined. Final *R* indices [$I>2\sigma(I)$]: $R_1=0.1120$, $wR_2=0.2991$.

Crystallographic data (excluding structure factors) for the structures in this paper have been deposited with the Cambridge Crystallographic Data Center as supplementary publication numbers CCDC-207851 and CCDC-207852. Copies of the data can be obtained, free of charge, on application to CCDC, 12 Union Road, Cambridge, CB2 1EZ, UK [fax: +44(0)-1223-336033 or e-mail: deposit@ccdc.cam.ac.uk].

Acknowledgements

Thanks are due to 'Région Haute-Normandie' via the Punch-Orga network for financial support to this project, including the thesis grant of A. Grandeury. CRIHAN is acknowledged for providing access to molecular modeling softwares. We also thank Dr. Loïc Toupet (UMR 6626, University of Rennes I, France) for crystal structure determinations.

References

1. Saenger, W. *Angew. Chem., Int. Ed. Engl.* **1980**, *19*, 344–362.
2. Szejtli, J. *Chem. Rev.* **1998**, *98*, 1743–1753.

3. Saenger, W.; Jacob, J.; Gessler, K.; Steiner, T.; Hoffmann, D.; Sanbe, H.; Koizumi, K.; Smith, S. M.; Takaha, T. *Chem. Rev.* **1998**, *98*, 1787–1802.
4. Rekharsky, M. V.; Inoue, Y. *Chem. Rev.* **1998**, *98*, 1875–1917.
5. Liu, L.; Guo, Q.-X. *J. Incl. Phenom. Macrocycl. Chem.* **2002**, *42*, 1–14.
6. Hedges, A. R. *Chem. Rev.* **1998**, *98*, 2035–2044.
7. Wenz, G. *Angew. Chem., Int. Ed. Engl.* **1994**, *33*, 803–822.
8. Rauf Khan, A.; Forgo, P.; Stine, K. J.; D'Souza, V. T. *Chem. Rev.* **1998**, *98*, 1977–1996.
9. Lipkowitz, K. B.; Coner, R.; Peterson, M. A. *J. Am. Chem. Soc.* **1997**, *119*, 11269–11276.
10. Cramer, F.; Dietsche, W. *Chem. Ber.* **1959**, *92*, 378–384.
11. Benschop, H. P.; Van den Berg, G. R. *J. Chem. Soc., Chem. Commun.* **1970**, 1435–1436.
12. Mikolajczyk, M.; Drabowicz, J. *J. Am. Chem. Soc.* **1978**, *100*, 2510–2515.
13. Kano, K.; Yoshiyasu, K.; Hashimoto, S. *J. Chem. Soc., Chem. Commun.* **1989**, 1278–1279.
14. Yannakopoulou, K.; Mentzafos, D.; Mavridis, I. M.; Dandika, K. *Angew. Chem., Int. Ed. Engl.* **1996**, *35*, 2480–2482.
15. (a) Hamilton, J. A.; Chen, L. *J. Am. Chem. Soc.* **1988**, *110*, 4379–4391; (b) Hamilton, J. A.; Chen, L. *J. Am. Chem. Soc.* **1988**, *110*, 5833–5841.
16. Makedonopoulou, S.; Yannakopoulou, K.; Mentzafos, D.; Lamzin, V.; Popov, A.; Mavridis, I. M. *Acta Crystallogr., Sect. B* **2001**, *57*, 399–409.
17. Harata, K. *Chem. Rev.* **1998**, *98*, 1803–1827.
18. Kano, K.; Kato, Y.; Kodera, M. *J. Chem. Soc., Perkin Trans. 2* **1996**, 1211–1217.
19. Grandeury, A.; Tisse, S.; Gouhier, G.; Agasse, V.; Petit, S.; Coquerel, G. *Chem. Eng. Technol.* **2003**, *26*, 354–358.
20. Harata, K.; Uekama, K.; Otagiri, M.; Hirayama, F. *J. Incl. Phenom.* **1984**, *1*, 279–293.
21. Harata, K.; Uekama, K.; Otagiri, M.; Hirayama, F. *Bull. Chem. Soc. Jpn.* **1983**, *56*, 1732–1736.
22. Harata, K.; Uekama, K.; Imai, T.; Hirayama, F.; Otagiri, M. *J. Incl. Phenom.* **1988**, *6*, 443–460.
23. Harata, K.; Hirayama, F.; Arima, H.; Uekama, K.; Miyaji, T. *J. Chem. Soc., Perkin Trans. 2* **1992**, 1159–1166.
24. Mentzafos, D.; Mavridis, I. M.; Schenk, H. *Carbohydr. Res.* **1994**, *253*, 39–50.
25. Caira, M. R.; Griffith, V. J.; Nassimbeni, L. R.; van Oudtshoorn, B. *J. Incl. Phenom.* **1995**, *20*, 277–290.
26. Brown, G. R.; Caira, M. R.; Nassimbeni, L. R.; van Oudtshoorn, B. *J. Incl. Phenom.* **1996**, *26*, 281–294.
27. Caira, M. R.; Griffith, V. J.; Nassimbeni, L. R.; van Oudtshoorn, B. *J. Chem. Soc., Perkin Trans. 2* **1994**, 2071–2072.
28. Caira, M. R.; Griffith, V. J.; Nassimbeni, L. R.; van Oudtshoorn, B. *Supramol. Chem.* **1996**, *7*, 119–124.
29. Rontoyianni, A.; Mavridis, I. M.; Israel, R.; Beurskens, G. *J. Incl. Phenom.* **1998**, *32*, 415–428.
30. Cardinael, P.; Peulon, V.; Perez, G.; Coquerel, G.; Toupet, L. *J. Incl. Phenom. Macrocycl. Chem.* **2001**, *39*, 159–167.
31. Gervais, C.; Beilles, S.; Cardinael, P.; Petit, S.; Coquerel, G. *J. Phys. Chem. B* **2002**, *106*, 646–652.
32. Schurig, V.; Jung, M.; Schmalzing, D.; Schleimer, M.; Duvekot, J.; Buyten, J. C.; Peene, J. A.; Mussche, P. *J. High Resolut. Chromatogr.* **1990**, *13*, 470–474.
33. Polavarapu, P. L.; Fontana, L. P.; Smith, H. E. *J. Am. Chem. Soc.* **1986**, *108*, 94–99.
34. Sheldrick, G. M. SHELX-97, University of Göttingen, Germany, 1997.
35. Stewart, J. J. P. MOPAC 93.00 Manual, Fujitsu Limited, Tokyo, Japan, 1993.
36. Mayo, S. L.; Olafson, B. D.; Goddard, W. A., III *J. Phys. Chem.* **1990**, *94*, 8897–8909.